



## The Simulation of Long-Range Transport of Biomass Burning Plume and Short-Range Transport of Anthropogenic Pollutants to a Mountain Observatory in East Asia during the 7-SEAS/2010 Dongsha Experiment

Ming-Tung Chuang<sup>1\*</sup>, Joshua S. Fu<sup>2</sup>, Chung-Te Lee<sup>3</sup>, Neng-Huei Lin<sup>4</sup>, Yang Gao<sup>2†</sup>,  
Sheng-Hsiang Wang<sup>4</sup>, Guey-Rong Sheu<sup>4</sup>, Ta-Chih Hsiao<sup>3</sup>, Jia-Lin Wang<sup>5</sup>,  
Ming-Cheng Yen<sup>4</sup>, Tang-Huang Lin<sup>6</sup>, Narisara Thongboonchoo<sup>7</sup>

<sup>1</sup> Graduate Institute of Energy Engineering, National Central University, Chung-Li 32001, Taiwan

<sup>2</sup> Department of Civil and Environmental Engineering, University of Tennessee, Knoxville, TN, USA

<sup>3</sup> Graduate Institute of Environmental Engineering, National Central University, Chung-Li 32001, Taiwan

<sup>4</sup> Graduate Institute of Atmospheric Physics, National Central University, Chung-Li 32001, Taiwan

<sup>5</sup> Department of Chemistry, National Central University, Chung-Li 32001, Taiwan

<sup>6</sup> Center for Space and Remote Sensing Research, National Central University, Chung-Li 32001, Taiwan

<sup>7</sup> College of Chemical Engineering, King Mongkut's Institute of Technology, Bangkok, Thailand

### ABSTRACT

The Community Multi-scale Air Quality Model (CMAQ) is used to simulate the long-range transport of biomass burning (BB) pollutants from Southeast Asia (SEA) towards the Taiwan Central Mountain Range (CMR) in March and April 2010. The results show that a proportion of the BB plume was blocked and compressed at the windward side of CMR. High-altitude BB plume is shown to influence air quality on the ground via three mechanisms: (1) the subsidence in the anticyclone, (2) the downward motion in the cold surge, and (3) the vertical mixing of the boundary layer over land. Two case studies are further investigated to probe the chemical evolution of the air parcel approaching Mt. Lulin. The first case shows that the third mechanism also explained the increase in the concentrations of peroxyacetyl nitrate (PAN), higher peroxyacetyl nitrate (PANX), NH<sub>3</sub>, SO<sub>2</sub>, and volatile organic compounds in the BB plume when entering the land over western Taiwan. Meanwhile, the percentage of NO<sub>3</sub><sup>-</sup> in the plume is also significantly increased. The second case reveals that valley wind transported air pollutants from the ground to the mountains. The air parcel, accompanied with considerable concentrations of PAN, PANX, SULF, and anthropogenic secondary organic aerosol, moved up Mt. Lulin. The pollutant concentrations, except for elemental carbon, in the air parcel decreased on approach to Mt. Lulin because the air parcel was mixed with a clean air.

**Keywords:** Biomass burning; Lulin high-mountain site; Simulation; 2010 Dongsha experiment.

### INTRODUCTION

The Southeast Asian (SEA) biomass burning (BB) has resulted in the impact in the downwind areas. For example, high ozone levels were observed at 2.5 km to 6.0 km in the troposphere above Hong Kong from the end of February to

the middle of April in 1994 and the trajectory of the overhead ozone plume was found to be traced back to Myanmar, where widespread fire spots occurred at the time (Chan *et al.*, 2000). Similar BB plumes were observed at 1,500 m at Doi Ang Khang (DAK) in northwestern Thailand by Aerosol Robotic Network (Sayer *et al.*, 2016). Hyer and Chew (2010) utilized the U.S. Navy Aerosol Aerosol and Prediction System (NAAPS, Zhang *et al.*, 2008) to simulate PM<sub>10</sub> (particulate matter with an aerodynamic diameter of < 10 μm) events in Singapore and Malaysia in September and October 2006 and indicated that high level of PM<sub>10</sub> exceeding 150 μg m<sup>-3</sup> is caused by the SEA BB. Nam *et al.* (2010) applied the results of GEOS-Chem (Goddard Earth Observing System Chemical Transport) model combined with satellite observations obtained using the Moderate Resolution Imaging Spectroradiometer (MODIS,

<sup>†</sup> Now at Atmospheric Science and Global Change Division, Pacific Northwest National Laboratory, Richland, Washington, 99352, USA

\* Corresponding author.

Tel.: +886-3-4227151 ext. 34665; Fax: +886-3-4226551

E-mail address: mtchuang100@gmail.com

King *et al.*, 1997), and illustrated that the SEA BB can cross the Pacific Ocean and reach North America. The community multi-scale air quality (CMAQ) model was applied to simulate the outflow from Asia to the Pacific and it is found that black carbon in the outflow originated not only from the anthropogenic sources of China and BB in Siberia and Kazakhstan from April to July, but also from the BB emissions of SEA and South China from February to April during 2008–2010 (Matsui *et al.*, 2013).

In recent years, several studies utilized air quality models to investigate the transport of SEA BB downwind to East Asia and western Pacific Ocean (Fu *et al.*, 2012; Huang *et al.*, 2013; Wang *et al.*, 2013; Wai and Tanner, 2014). These studies mainly related to regional transport. The impact of the SEA BB on Taiwan/Mt. Lulin has previously been investigated (Sheu *et al.*, 2010; Lee *et al.*, 2011; Fu *et al.*, 2012; Ou-Yang *et al.*, 2012; Huang *et al.*, 2013; Chuang *et al.*, 2014; Chang *et al.*, 2013; Lin *et al.*, 2014; Chuang *et al.*, 2015). In contrast, the mesoscale/microscale understanding of how the BB plumes are transported to Taiwan remains partially understood.

In addition to long-range transport of BB pollutants, the short-range transport of anthropogenic pollutants should be considered for air quality issues. Ground pollutants can be transported to mountains via valley wind (Carnuth and Trickl, 2000; Frioud *et al.*, 2003; Marinoni *et al.*, 2010). Baltensperger *et al.* (1997) used a convection model to simulate valley wind to explain the transport of aerosol from the ground to mountains, resulting in high aerosol concentrations observed at the high-alpine site Jungfraujoch (3450 m). Exposed to daytime thermal effects, the valley wind blows along the slope from the ground to the mountains. By contrast, mountain wind blows along the slope from the high mountains to the ground during nighttime. Therefore, the CO (Lin *et al.*, 2010) and Hg (Sheu *et al.*, 2010) pollutants vary in a diurnal cycle at Mt. Lulin, which also implies that thermal circulation can transport pollutants between ground and mountain top.

Observational studies conducted at high mountain sites usually aim to determine whether pollutants reach these sites through long-range transport or short-range transport (Marinoni *et al.*, 2010; Ou Yang *et al.*, 2012; Perrone *et al.*, 2012; Zhang *et al.*, 2014). For the experiments conducted at Mt. Lulin, the question is whether the BB plume moves from the foot of mountains, horizontally at almost the same altitude of Mt. Lulin, or from an altitude lower than Mt. Lulin and then vertically upward along the slope (Lee *et al.*, 2011; Chuang *et al.*, 2014). Therefore, the purpose of the present study is to simulate how the long-range transport of BB pollutants and short-range transport of anthropogenic sources approached Mt. Lulin in March and April 2010 and to address above questions. Besides, the present study estimated the influence of BB pollutants on surface air quality.

## METHODS

### *Model Description and Configuration*

The CMAQ model (Byun and Schere, 2006) was used to

simulate the chemical reactions of pollutants. In this model, meteorological data provided by the weather research and forecasting (WRF) model (Wang *et al.*, 2012) and emission data included anthropogenic emissions from Intercontinental Chemical Transport Experiment–Phase B (INTEX-B; Zhang *et al.*, 2009), biogenic emissions from Model of Emission of Gases and Aerosol from Nature (MEGAN; Guenther *et al.*, 2012), and BB smoke emissions from the Fire Locating and Modeling of Burning Emissions (FLAMBE; Reid *et al.*, 2009).

In the present study, the FLAMBE emissions are processed as described by Fu *et al.* (2012), Huang *et al.* (2013), and Chuang *et al.* (2015). Fu *et al.* (2012) applied the emission factor table in Andreae and Merlet (2001) to estimate emission of different species ( $\text{SO}_2$ ,  $\text{NO}_2$ , NO, CO, BC, OC,  $\text{NH}_3$ ,  $\text{CH}_4$ , NMHCs, and  $\text{PM}_{2.5}$ ). The injection heights of biomass burning emission are set according to the parameterization and look-up table in Air Sciences, Inc. (2002). Chuang *et al.* (2015) conducted a series of sensitivity tests for the FLAMBE inventory, and found that the BB emissions over SEA may be overestimated by a factor of 4. Therefore, the BB emission was reduced by 75% in the present study.

The anthropogenic sources may have been underestimated in the 2010 simulation because the INTEX-B emission inventory was based on 2006, and emission increase from 2006 to 2010 due to economic growth was not accounted for. Since Taiwan has developed its own emission inventory, the anthropogenic ( $\text{NO}_x$ ,  $\text{SO}_x$ , CO, total suspended particulates,  $\text{PM}_{10}$ ,  $\text{PM}_{2.5}$  (particulate matter with aerodynamic diameters of less than 10 and 2.5  $\mu\text{m}$ , respectively), and total hydrocarbons) and biogenic sources for Taiwan domain (innermost domain in Fig. 1) was replaced by the updated Taiwan Emission Data System version 7.1 (TEDS7.1; Taiwan Environmental Protection Agency, 2011). The sparse matrix operator kernel emission system (SMOKE; Houyoux and Vukovich, 1999) converts TEDS7.1 into inputs for the CMAQ simulation. Although TEDS7.1 was based on 2007 data, the emission growth was reasonably stagnant, because the economic increase from 2007 to 2010 was negligible (Lau, 2012).

The model configuration used in the present study is described by Chuang *et al.* (2015). The domain1, 2, 3 were a set of three nested domains with horizontal resolutions of 45, 15, and 5 km (Fig. 1). Although Chuang *et al.* (2015) and the present study used the same model configuration, it is noted that Chuang *et al.* (2015) analyzed the simulation of domain 2, while the analysis in the present was performed using domain 3. Since CMAQ is an Eulerian model, we cannot get the information of chemical evolution of pollutants in the BB plume along the moving trajectories. Therefore, the HYSPLIT model (Draxler and Rolph, 2013) is applied to record the location of BB plume.

In domain 3, the Central Mountain Range (CMR) covers northeast to southwest of Taiwan (Fig. 1). Mt. Lulin is located in the CMR in central Taiwan. The simulation period was from March to April 2010. In order to evaluate the influence of BB pollutants on surface air quality, two simulations were executed: (1) the BASE case involving BB and non-

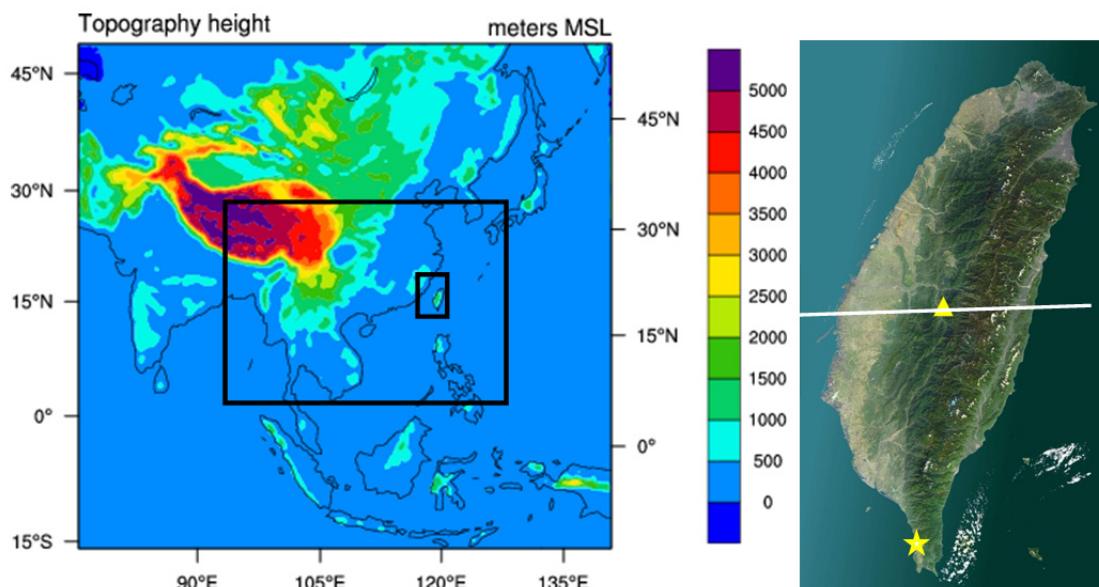


**Fig. 1.** Three nested domains for current simulation and the map of Taiwan (All the mountains across Taiwan is collectively called the Central Mountain Ranges, CMR. The yellow triangle and yellow star indicate the location of Mt. Lulin and Hengchun sites, respectively). The white line across CMR and Mt. Lulin site will be illustrated as the cross-section of PM<sub>2.5</sub> plume in Figs. 4 and 6.

BB emissions and (2) the non-BB case excluding the BB emissions. The difference between these two simulations is then the impact of BB pollutants. The remaining in (1) excluding the impact of BB is the impact of non-BB pollutants. In the BASE case, 12 events were observed with Mt. Lulin site at PM<sub>10</sub> > 35  $\mu\text{g m}^{-3}$  and CO > 0.3 ppm preconditions: 12 March 03:00 LST, 12 March 16:00 LST; 16 March 18:00 LST; 18 March 01:00 LST; 21 March 08:00 LST; 25 March 17:00 LST; 26 March 05:00 LST; 28 March 06:00 LST; 5 April 19:00 LST; 6 April 19:00 LST; 11 April 03:00 LST; and 11 April 16:00 LST. The case studies (12 March 2010 16:00 LST and 6 April 2010 19:00 LST) are selected as in Chuang *et al.* (2015) for the two events to illustrate the impact of the BB plume on air quality in Taiwan. The results and discussions in the present study showed that the high resolution simulation results resolved detailed transport mechanism when the long-range transport of BB plume and short-range transport of surface anthropogenic sources approach Mt. Lulin on a mesoscale/microscale scale, which could not be resolved by the simulation results of domain 2 in Chuang *et al.* (2015).

The observations from Mt. Lulin and the ground site of Hengchun ground site (Fig. 1) were considered and compared with the simulation results. Mt. Lulin (2,862 m) is located in central Taiwan and is suitable to observe the background atmosphere downwind of East Asia (EA) and SEA, since Mt. Lulin is usually on the downwind path of high-atmosphere westerlies. The Hengchun site was chosen to assess the air pollutant concentrations on the ground. It is located at the southern tip of Taiwan and is less influenced by the anthropogenic sources that are mainly distributed on the western side of Taiwan. The air quality in Hengchun is mainly influenced by the local pollution and the background atmosphere from the east of Taiwan or the west Pacific.

Therefore, the Hengchun site is suitable to observe the near-surface background atmosphere and to assess the impact of high-altitude BB plume on the surface air quality.

#### Model Simulation Performance

Before analyzing the simulation results, the performance of model simulation should be evaluated such that the analysis is persuasive. In this study, the simulations and observations at the Mt. Lulin and Hengchun site both also compared (Table 1 and Fig. 2). The simulation performances of O<sub>3</sub> in Mt. Lulin and Hengchun were comparable. The simulation performances of CO and PM<sub>10</sub> in Hengchun were slightly less satisfactory than those in Mt. Lulin. This finding indicates that Hengchun is on the surface and more influenced by anthropogenic source than the mountain site Mt. Lulin. Although the indexes of agreement of CO and PM<sub>10</sub> were 0.55 and 0.50 in Hengchun, the performance remained reliable (Willmott, 1981). The benchmarks of the mean fractional bias and mean fractional error of O<sub>3</sub> are 15% and 35%, respectively, while the benchmarks of the mean fractional bias and mean fractional error of PM were 50% and 75%, respectively (United States Environmental Protection Agency, 2007). Therefore, the simulation performance of O<sub>3</sub> in the present study is good whereas the simulation performance of PM is acceptable (Table 1). The trend of simulations and observations of PM<sub>10</sub> in the first half of March and the second half of April were acceptable. By contrast, the trend of simulations and observations in the second half in March and the first half in April was underestimated (Fig. 2(c)). In addition, the sampling of PM<sub>2.5</sub> from March 12 to March 31 and from April 10 to April 22 (Lin *et al.*, 2013) were compared with that of the simulations (Fig. 2(d)). The simulated PM<sub>2.5</sub> elemental carbon (EC) concentrations was satisfactory in comparison to observations

**Table 1.** Statistics of observed and simulated CO, O<sub>3</sub>, and PM<sub>10</sub> at Mt. Lulin and Hengchun sites.

| Pollutants | Mt. Lulin |                |                  | Hengchun |                |                  |                   |
|------------|-----------|----------------|------------------|----------|----------------|------------------|-------------------|
|            | CO        | O <sub>3</sub> | PM <sub>10</sub> | CO       | O <sub>3</sub> | PM <sub>10</sub> | PM <sub>2.5</sub> |
| RMSE       | 91.87     | 11.83          | 16.05            | 123.65   | 11.83          | 23.68            | 11.66             |
| MNB        | -0.22     | 0.05           | -0.02            | -0.42    | 0.11           | -0.28            | -0.36             |
| MNE        | 0.35      | 0.20           | 0.77             | 0.43     | 0.25           | 0.56             | 0.62              |
| MFB        | -0.32     | 0.01           | -0.45            | -0.57    | 0.06           | -0.55            | -0.70             |
| MFE        | 0.42      | 0.18           | 0.77             | 0.58     | 0.21           | 0.71             | 0.83              |
| IOA        | 0.74      | 0.67           | 0.65             | 0.55     | 0.67           | 0.50             | 0.62              |
| F2[0.5,2]  | 0.79      | 0.99           | 0.50             | 0.62     | 0.97           | 0.50             | 0.40              |
| R          | 0.66      | 0.52           | 0.44             | 0.52     | 0.53           | 0.32             | 0.47              |

Note: the formulas of above statistical parameters RMSE: Root Mean Square Error; MNB: Mean Normalized Bias; MNE: Mean Normalized Gross Error; MFB: Mean Fractional Bias; MFE: Mean Fractional Gross Error, IOA: Index of Agreement; F2: Factor 2; R: Correlation coefficient. The formulas for these statistical parameters can refer to Appendix A in Fu *et al.* (2012). There is no PM<sub>2.5</sub> hourly measurement for the period of study at Mt. Lulin site.

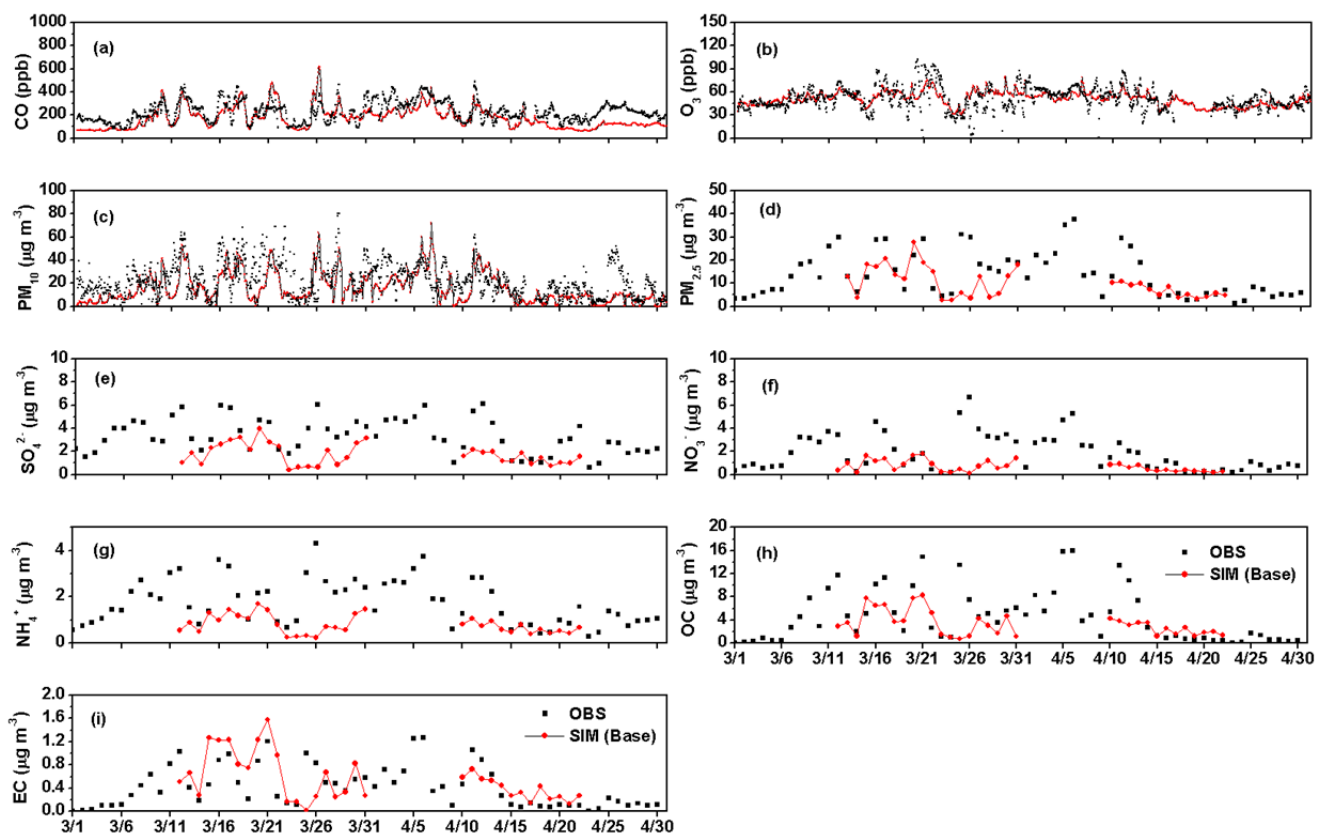


**Fig. 2.** The comparison of hourly observed and simulated (a) CO, (b) O<sub>3</sub>, (c) PM<sub>10</sub> and daily observed and simulated (d) PM<sub>2.5</sub>, (e) SO<sub>4</sub><sup>2-</sup>, (f) NO<sub>3</sub><sup>-</sup>, (g) NH<sub>4</sub><sup>+</sup>, (h) OC, (i) EC at Mt. Lulin site. The daily average ranges between 08:00 LST to 08:00 LST.

(Fig. 2(i)), but the concentrations of other simulated PM<sub>2.5</sub> compositions were underestimated (Figs. 2(e)–2(h)). The reason is that the 5 Km resolution cannot resolve the complex terrain and thus wind speed was overestimated and PM<sub>2.5</sub> concentrations was overly diluted (not shown).

## RESULTS AND DISCUSSION

### Impact of PM<sub>2.5</sub> from BB and Non-BB Emissions

The quantitative contribution of specific sources to

mountain areas, e.g., Asian dust and anthropogenic sources to Yang-Ming mountain located in northern Taiwan (Lin *et al.*, 2004), pesticide to Southern Alps of New Zealand (Lavin and Hageman, 2013), has rarely been estimated. For Mt. Lulin, the contribution of SEA BB pollutants is expected to be evident during spring time. Also, anthropogenic local pollution in western Taiwan, can be transported upward via the valley wind, particularly in the afternoon, or via the elevation of boundary layer over western Taiwan during daytime (Sheu *et al.*, 2010; Lee *et al.*, 2011; Ou-Yang *et*

al., 2012; Chuang et al., 2014).

In the 12 events described previously, the contributions of PM<sub>2.5</sub> from the BB emissions accounted for approximately 60% to 90% of total PM<sub>2.5</sub> concentrations when Mt. Lulin was surrounded by the BB plume (Fig. 3). Besides, these events, the BB emissions influenced Mt. Lulin most of the time, except in the last two weeks of April 2010. At the same time, Mt. Lulin was influenced by non-BB sources, but the impact on air quality was reduced during the event periods. The average contributions of BB and non-BB emissions in the simulated PM<sub>2.5</sub> at Mt. Lulin were 53% and 47%, respectively, except those obtained in the first seven days in March 2010 because the impact of the initial condition decayed with the simulation time. However, the influence of BB emissions was stronger in March 2010 than in April 2010 (Fig. 3). The impact of the BB emissions was reduced in the second half of April 2010. The contributions of BB and non-BB emissions were 16% and 84%, respectively, from April 16 to April 30, 2010. This finding follows the peak of the SEA BB activity in March 2010 and the subsequent decline in April 2010 as observed by Yen et al. (2013).

### **BB Plume Approaching Mt. Lulin**

#### *BB Event on 12 March 2010, 16:00 LST*

The cross section of the white straight line indicated in Fig. 1) was shown in Fig. 4. On 11 March 2010 at 10:00 LST, the simulated PM<sub>2.5</sub> at Mt. Lulin was comparable to the surrounding troposphere at less than 10  $\mu\text{g m}^{-3}$  (Fig. 4(a)). The BB and non-BB emissions accounted for 24% and 76% of the simulated PM<sub>2.5</sub>, respectively (Fig. 3). The BB plume of the simulated PM<sub>2.5</sub> ranged from 10  $\mu\text{g m}^{-3}$  to 20  $\mu\text{g m}^{-3}$  and covered 2 km to 4 km over western Taiwan. The BB plume height was simulated well since observations appealed a mean height of 3 km (Lee et al., 2016a). The BB plume did not visibly influence Mt. Lulin or CMR. Another zone with high PM<sub>2.5</sub> was found in the inland area near the bottom of the western mountains, and this value ranged from 40  $\mu\text{g m}^{-3}$  to 50  $\mu\text{g m}^{-3}$  (Fig. 4(a)). At 12:00

LST, the high-altitude BB plume reached Mt. Lulin. The PM<sub>2.5</sub> plume from 12:00 LST to 16:00 LST in the inland area moved along the slope from the bottom of the CMR to Mt. Lulin, where the simulated PM<sub>2.5</sub> was only 20  $\mu\text{g m}^{-3}$  to 30  $\mu\text{g m}^{-3}$ . The BB and non-BB emissions accounted for 28% and 72% of the total simulated PM<sub>2.5</sub>, respectively. Therefore, the simulated PM<sub>2.5</sub> was from the sources at the bottom of the CMR.

At 22:00 LST on March 11, the high value of simulated PM<sub>2.5</sub> BB plume reached Mt. Lulin. When the BB plume approached the windward side of the CMR, the simulated PM<sub>2.5</sub> of 10  $\mu\text{g m}^{-3}$  to 20  $\mu\text{g m}^{-3}$  increased to 20  $\mu\text{g m}^{-3}$  to 30  $\mu\text{g m}^{-3}$  at Mt. Lulin because the plume was compressed and concentrated. The BB and non-BB emissions accounted for 65% and 35% of the total simulated PM<sub>2.5</sub>, respectively; this result indicated that the high-altitude BB plume was the main source of particulates in Mt. Lulin. The BB plume reached Mt. Lulin at 08:00 LST on March 11, and the observed PM<sub>10</sub> reached 55  $\mu\text{g m}^{-3}$  (Fig. 2(c)). The simulated PM<sub>10</sub> and PM<sub>2.5</sub> were 53 and 46  $\mu\text{g m}^{-3}$  at 03:00 LST on March 12, respectively. The high-altitude BB plume was continuously blocked and compressed at the windward side of the CMR from 23:00 LST on March 11 to 04:00 LST on March 12 (Figs. 4(g)–4(k)). The blocking forced the BB plume to move very slowly at the west side of the CMR. The BB in the simulated PM<sub>2.5</sub> also increased from 70% to 81% in Mt. Lulin. The BB plume, which was above 1.5 km, gradually subsided along the west side of the CMR to the ground and gradually distributed at the west of the CMR from a high altitude to the ground. The simulated PM<sub>2.5</sub> remained at 30  $\mu\text{g m}^{-3}$  to 40  $\mu\text{g m}^{-3}$  on the windward side of the CMR until the next morning.

Although the CMR blocked the transport of the simulated BB plume, a part of the BB plume at approximately the height of CMR or higher crossed over the CMR and transported to the Pacific. Therefore, the simulated PM<sub>2.5</sub> in Mt. Lulin decreased. The observed PM<sub>10</sub> of 62  $\mu\text{g m}^{-3}$  decreased at 10:00 LST on March 12 (Fig. 2(c)). At 10:00

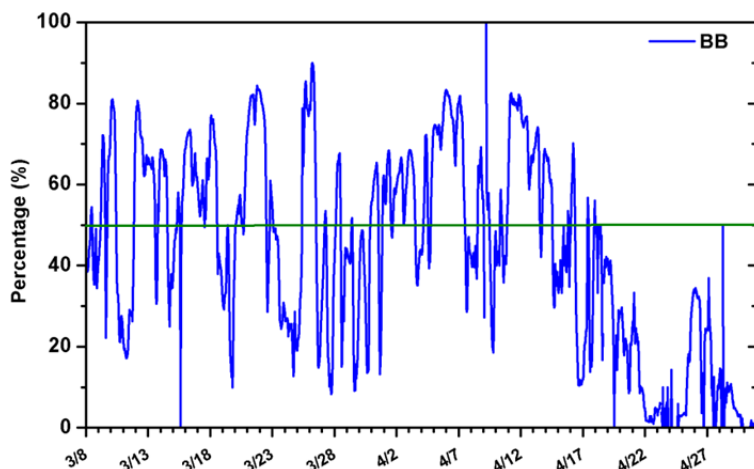


**Fig. 3.** The proportion of PM<sub>2.5</sub> from biomass burning (BB) and non-biomass burning (nonBB) on Mt. Lulin, respectively. PM<sub>2.5</sub> for BB is equal to simulated PM<sub>2.5</sub> in BASE case minus that in nonBB case. PM<sub>2.5</sub> for nonBB is the simulated PM<sub>2.5</sub> in nonBB case. The arrows indicate the occurrence of the 12 events with PM<sub>10</sub> > 35  $\mu\text{g m}^{-3}$  and CO > 0.3 ppm except two events discussed in present study are indicated by dashed line arrows.

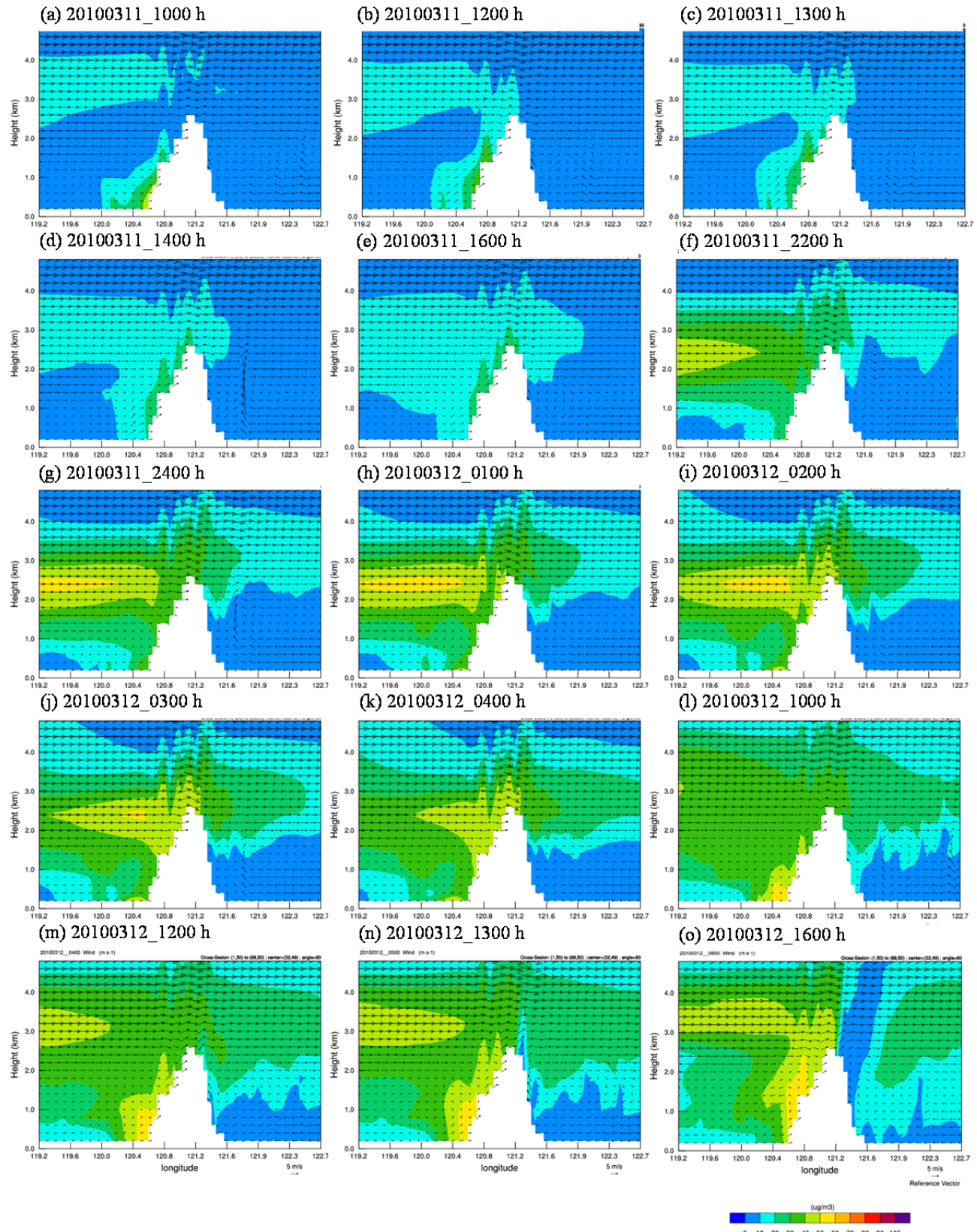


**Fig. 4.** The simulated PM<sub>2.5</sub> contour and wind field of the vertical section A-A in Fig. 1 at (a) 10:00 LST on March 11, (b) 12:00 LST on March 11, (c) 13:00 LST on March 11, (d) 14:00 LST on March 11, (e) 16:00 LST on March 11, (f) 22:00 LST on March 11, (g) 24:00 LST on March 11, (h) 1:00 LST on March 12, (i) 2:00 LST on March 12, (j) 3:00 LST on March 12, (k) 4:00 LST on March 12, (l) 10:00 LST on March 12, (m) 12:00 LST on March 12, (n) 13:00 LST on March 12, and (o) 16:00 LST on March 12 2010, respectively.

LST on March 12, the simulated  $\text{PM}_{2.5}$  reduced from  $50 \mu\text{g m}^{-3}$  to below  $40 \mu\text{g m}^{-3}$  (Fig. 4(l)), and the proportion of the BB in the simulated  $\text{PM}_{2.5}$  decreased from 81% to 72%. At 16:00 LST, the proportion of BB and non-BB in the simulated  $\text{PM}_{2.5}$  reduced from 72% to 63% and increased from 28% to 37%, respectively. The simulated  $\text{PM}_{2.5}$  parcel in the inland area was transported again from the bottom along the slope of the CMR to Mt. Lulin and even combined with the high-altitude BB plume at 16:00 LST on March 12 (Figs. 4(l)–4(n)). The vertical gradient of the simulated  $\text{PM}_{2.5}$  concentration was very small (Figs. 4(l) and 4(m)) and reached below 1.3 km over west Taiwan during daytime. This finding indicated that the vertical mixing in the boundary layer was strong on this day and favored the influence of high-altitude BB plume on the air quality near the surface.

In the daytime on March 11, the simulated high-altitude BB plume and the simulated  $\text{PM}_{2.5}$  plume near the ground did not mix (Figs. 4(a)–4(e)). Since the early morning of March 12, the high-altitude BB plume subsided to a lower portion of the atmosphere and mixed with the  $\text{PM}_{2.5}$  plume near the ground (Figs. 4(g)–4(o)). Although Taiwan was located in the anticyclone on the surface and at 700 hPa weather maps on both March 11 and March 12, 2010, Taiwan was still in the anticyclone on March 12 at 850 hPa (Fig. 5). In other words, the subsidence on March 12 was stronger than that on March 11. Therefore, the high-altitude BB plume easily subsided to the ground and influenced air quality near the surface. Similar subsidence was simulated by Fu *et al.* (2012).

#### *BB Event on 6 April 2010, 19:00 LST*

At 13:00 LST on April 5, the air quality at Mt. Lulin was mainly influenced by the high-altitude simulated BB plume, and the simulated  $\text{PM}_{2.5}$  ranged from  $20 \mu\text{g m}^{-3}$  to  $30 \mu\text{g m}^{-3}$  (Fig. 6(a)). The proportions of the BB and non-BB in the simulated  $\text{PM}_{2.5}$  were 70% and 30%, respectively. As the BB plume approached the CMR, the BB plume entered the Pacific anticyclone and subsided gradually. The simulated  $\text{PM}_{2.5}$  at Mt. Lulin exceeded  $30 \mu\text{g m}^{-3}$  (Fig. 6(b)). The BB plume with the simulated  $\text{PM}_{2.5}$  of  $> 40 \mu\text{g m}^{-3}$  ranged from 2.5 km to 3.5 km at 15:00 LST but ranged from 2.3 km to 2.8 km at 19:00 LST. At 19:00 LST, the BB plume accounted for 83% of the simulated  $\text{PM}_{2.5}$  at Mt. Lulin. When the BB plume subsided to the height of Mt. Lulin, the simulated  $\text{PM}_{2.5}$  at Mt. Lulin also exceeded  $40 \mu\text{g m}^{-3}$ . The observed and simulated  $\text{PM}_{10}$  reached  $45 \mu\text{g m}^{-3}$  and  $56 \mu\text{g m}^{-3}$  at 16:00 LST and 19:00 LST, respectively (Fig. 2(c)). The high-altitude BB plume likely moved downward and possibly reached the ground because of the subsidence (Figs. 6(e) and 6(f)).

Later, the simulated  $\text{PM}_{2.5}$  at Mt. Lulin gradually decreased because the simulated BB plume subsided at the windward and leeward sides of the CMR. At 07:00 LST on April 6, the simulated  $\text{PM}_{2.5}$  decreased and reached  $< 30 \mu\text{g m}^{-3}$  (Fig. 6(h)). The proportion of the BB plume in the simulated  $\text{PM}_{2.5}$  decreased. Another BB plume moved to Mt. Lulin (Fig. 6(h)) and then compressed at the windward side of the CMR (Fig. 6(i)). However, at 10:00 LST, the proportion

of the BB plume decreased to 77% and even decreased to 65% at 17:00 LST because diluted by the less polluted  $\text{PM}_{2.5}$  plume from the ground to Mt. Lulin (Fig. 6(n)). Therefore, the compression was not evident during the daytime until 19:00 LST (Fig. 6(o)). The vertical gradient concentration of the simulated  $\text{PM}_{2.5}$  was very small from the ground to 1.3 km height on the west of the CMR from 10:00 LST to 15:00 LST (Figs. 6(i)–6(m)). This indicated that the strong turbulent mixing again helped the vertical transport of high altitude BB plume to the ground. The simulated BB plume approaching Mt. Lulin on April 6 did not subside as the simulated BB plume did on April 5 (Figs. 6(i)–6(l)). Taiwan was not in the anticyclone regardless of the upper or surface weather charts (Fig. 7). Therefore, the subsidence unlikely caused the downward transport of the high-altitude BB plume to the ground. However, a front passed Taiwan on April 5 (Fig. 7(c)). Yen *et al.* (2013) explained that the front accompanied with a cold surge forces high-altitude BB pollutants to the ground and influences the air quality near the surface. Therefore, the downward motion in the front/cold surge could be another mechanism of the subsidence of the high-altitude BB plume on April 5.

#### *Chemical Evolution of Plume Approaching Mt. Lulin*

In this section, we discuss the chemical evolution of  $\text{PM}_{2.5}$  plume along the moving trajectories arriving at Mt. Lulin for the two different events discussed in the last section.

#### *BB Plume from SEA*

On the basis of Fig. 4(j), we can determine that the plume influencing Mt. Lulin at 3:00 LST on March 12 was the BB plume via long-range transport, as illustrated by the background trajectory in Fig. 8(a). The BB plume was approximately 1,500 m to the southwest off the coast of Taiwan 25 h before the plume arrived at Mt. Lulin. At 10:00 LST on March 11, the BB plume was above land; at 14:00 LST, the BB plume turned to the north (turning point) and slowly climbed Mt. Lulin. The BB plume was blocked by the CMR and was compressed at the windward side of CMR. The plume in the rear pushed the BB plume forward. Then, the BB plume slowly approached the CMR, turned northeast, and arrived at Mt. Lulin.

We consider the chemical evolution of the BB pollutants along the trajectories. The simulated environmental variables, such as temperature, water vapor, and products, including  $\text{O}_3$ ,  $\text{PM}_{10}$ , and  $\text{PM}_{2.5}$ , did not noticeably vary in the BB plume as the plume approached the CMR. Initially, it seemed that the OM dominated in the BB plume before influenced by anthropogenic pollutants  $\text{SO}_4^{2-}$  (Lee *et al.*, 2016b). At 12:00 LST on March 11, the BB plume was over land (Figs. 9(a)–9(e)). Primary and secondary anthropogenic pollutants, such as  $\text{NH}_3$ ,  $\text{SO}_2$ , volatile organic compounds (VOCs), peroxyacetyl nitrate (PAN), and higher peroxyacetyl nitrate (PANX), and PANX, increased. The proportion of  $\text{NO}_3^-$  in  $\text{PM}_{2.5}$  also increased from 4% to 21% (Fig. 9(f)). As a result, the proportion of organic matter (OM) and EC decreased. The BB plume was initially influenced by the anthropogenic pollution from the ground in this event.

After 14:00 LST, the proportion of  $\text{NO}_3^-$  in  $\text{PM}_{2.5}$  began

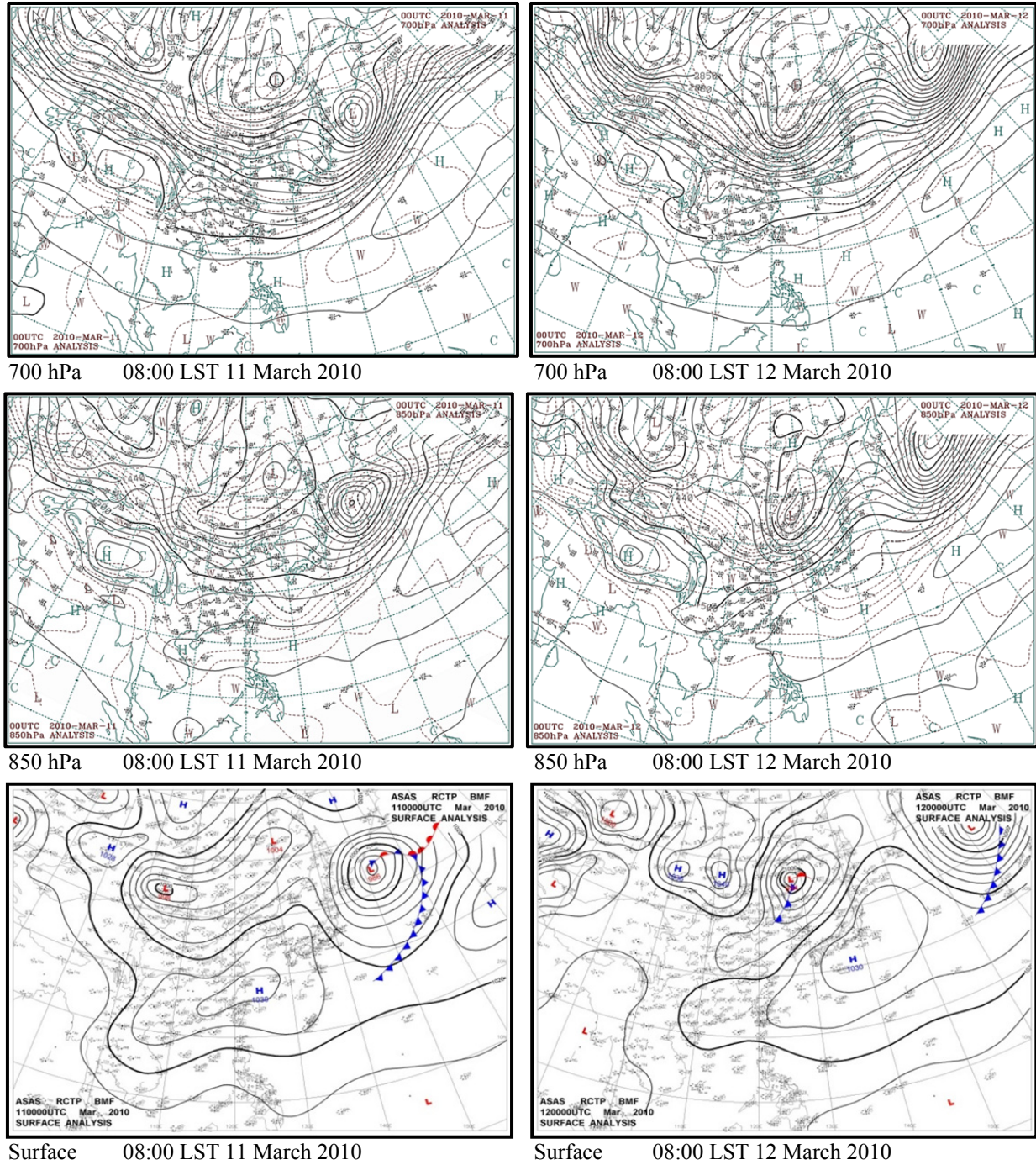


**Fig. 5.** The high altitude (700 LSTPa and 850 hPa) and surface weather map for 08:00 LST 11 March (left) and 08:00 LST 12 March (right) 2010, respectively.

to decreased. The proportion of  $\text{NO}_3^-$  in  $\text{PM}_{2.5}$  decreased from 21% to <10% from 14:00 LST to 22:00 LST on March 11. Meanwhile, the trend of  $\text{NO}_3^-$  concentration was consistent to the proportion of  $\text{NO}_3^-$  in  $\text{PM}_{2.5}$ . The proportion of OM and EC in  $\text{PM}_{2.5}$  relatively increased. This finding indicated that the BB plume approached the CMR from 14:00 LST to 22:00 LST, and the BB plume was compressed. This compression increased the  $\text{PM}_{2.5}$  concentration, as well as OM and EC in the BB plume. From Figs. 3 and 4, it indicates that the compression started when the BB plume

has reached Mt. Lulin. The compression would continue until the proportion of BB reached a peak, 05:00 LST on March 12. The proportion of  $\text{NO}_3^-$  in  $\text{PM}_{2.5}$  increased during the daytime of March 11 (Fig. 4(j)); this finding was attributed to the turbulent mixing in the boundary layer. The pollutants near the surface moved to a high altitude, particularly >1 km, and increased the  $\text{NO}_3^-$  concentration from <1  $\mu\text{g m}^{-3}$  to 4.3  $\mu\text{g m}^{-3}$  from 11:00 LST to 14:00 LST. After 14:00 LST, the  $\text{NO}_3^-$  concentration in the BB plume decreased to 2.8  $\mu\text{g m}^{-3}$  after the BB plume reached the

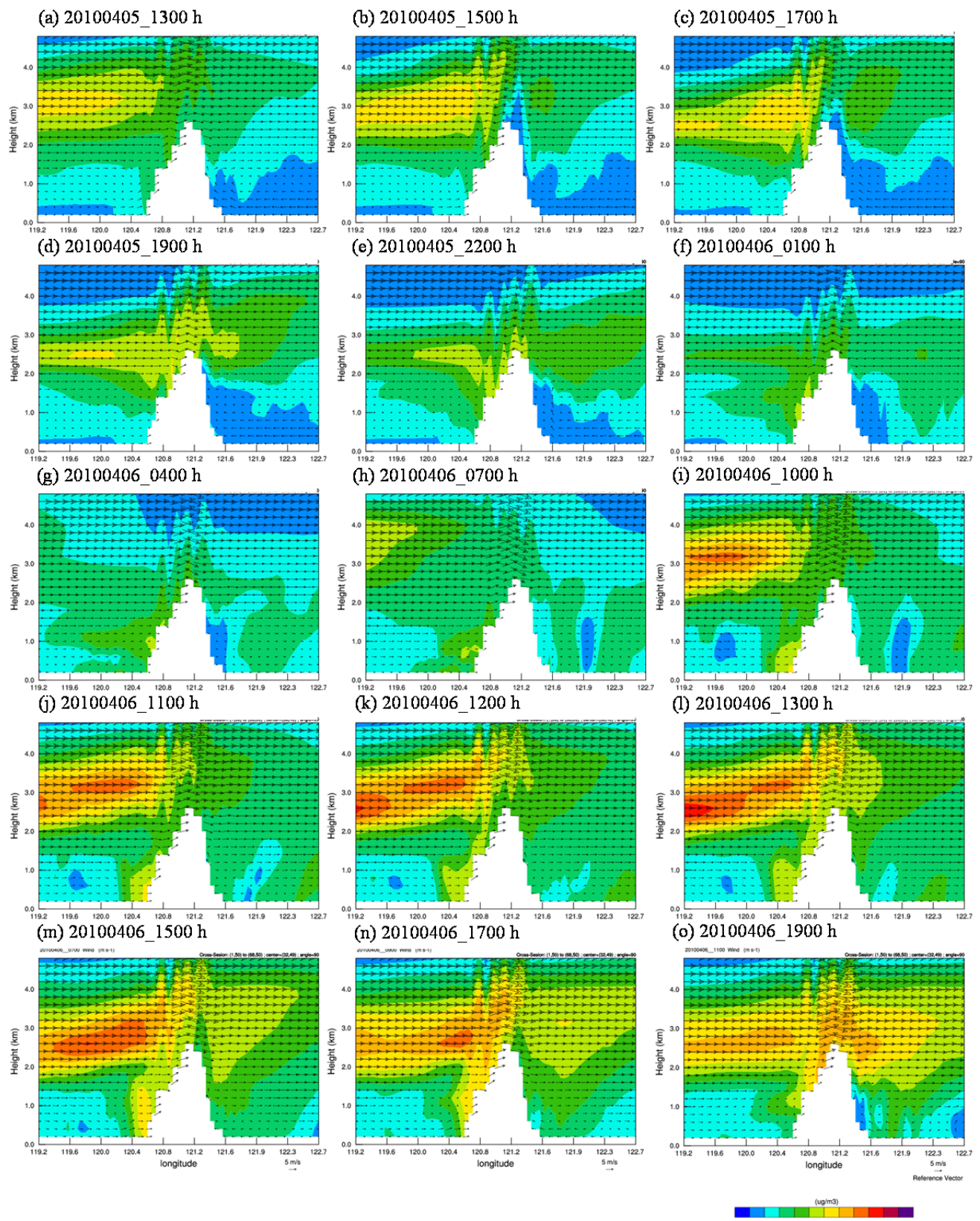


**Fig. 6.** The simulated PM<sub>2.5</sub> contour and wind field of the vertical section A-A in Figure 1 at (a) 13:00 LST. on April 5, (b) 15:00 LST. on April 5, (c) 17:00 LST. on April 5, (d) 19:00 LST on April 5, (e) 22:00 LST on April 5, (f) 1:00 LST on April 6, (g) 4:00 LST on April 6, (h) 7:00 LST on April 6, (i) 10:00 LST on April 6, (j) 11:00 LST on April 6, (k) 12:00 LST on April 6, (l) 13:00 LST on April 6, (m) 15:00 LST on April 6, (n) 17:00 LST on April 6, and (o) 19:00 LST on April 6 2010, respectively.

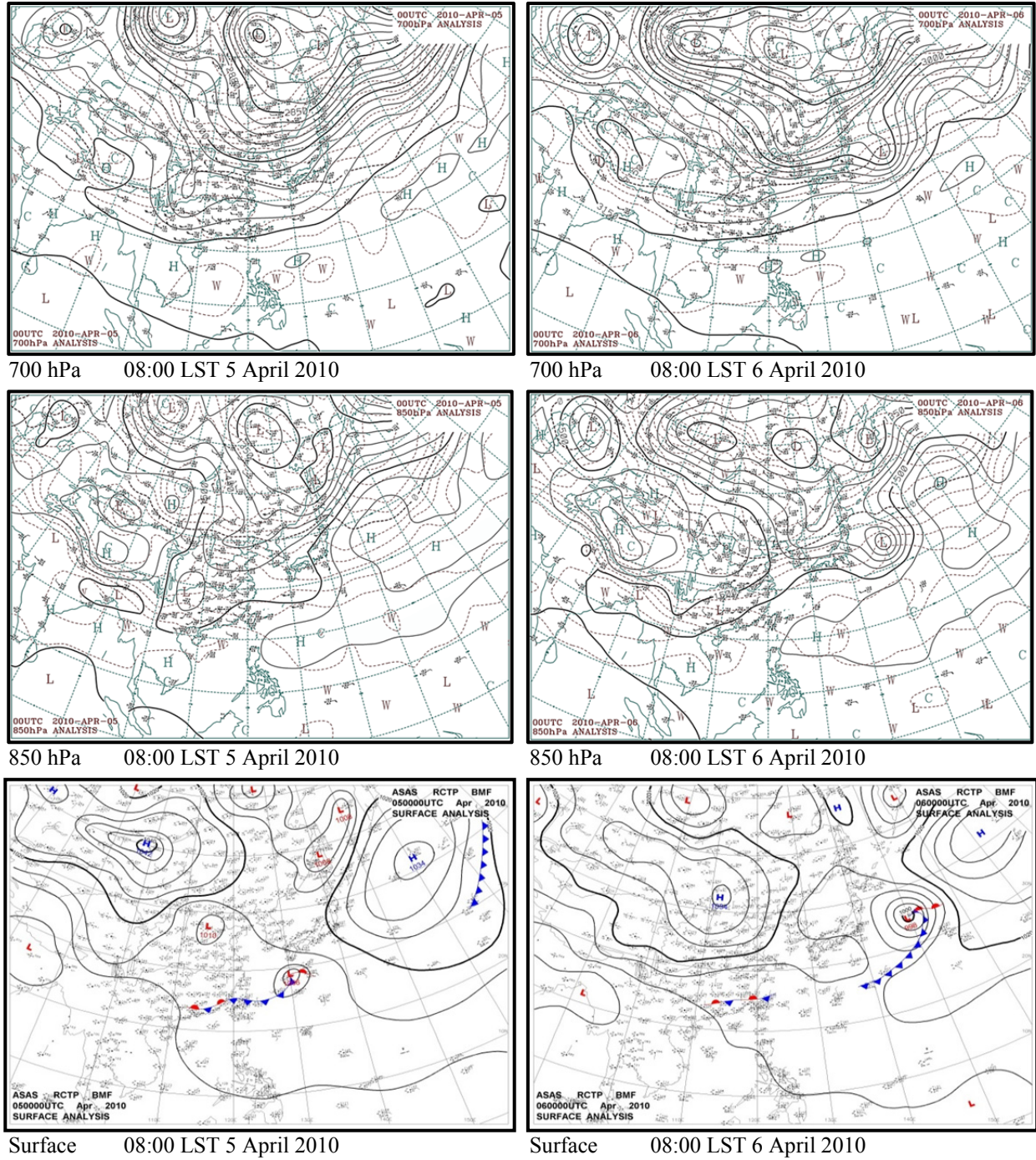


**Fig. 7.** The high altitude (700 LSTPa and 850 hPa) and surface weather map for 08:00 LST on April 5 (left) and 08:00 LST on April 6 (right) 2010, respectively.

turning point to the north at 22:00 LST. Meanwhile, the OM and EC increased from  $4.5 \mu\text{g m}^{-3}$  to  $9.3 \mu\text{g m}^{-3}$  and from  $0.5 \mu\text{g m}^{-3}$  to  $0.9 \mu\text{g m}^{-3}$ , respectively. This trend indicated that the influence from the near-surface anthropogenic pollutions decreased after 14:00 LST. The BB plume moved upward in the CMR from 1,500 m to 2,900 m from 22:00 LST on March 11 to 03:00 LST on March 12. The compression of the BB plume was more evident at this point than a few hours before this event occurred. The OM and EC increased from  $9.3 \mu\text{g m}^{-3}$  to  $19.4 \mu\text{g m}^{-3}$  and from

$0.9 \mu\text{g m}^{-3}$  to  $1.5 \mu\text{g m}^{-3}$ , respectively. The total inorganic ion concentration increased from  $15.9 \mu\text{g m}^{-3}$  to  $23.5 \mu\text{g m}^{-3}$ . In the final stage of the movement of the BB plume to Mt. Lulin, the BB plume started from 1,500 m at the windward side of the CMR and then gradually climbed to Mt. Lulin at approximately 2,900 m through terrain lifting, as illustrated in Fig. 8(a).

#### ***Anthropogenic Plume from the Ground***

The chemical evolution of pollutants along the trajectory

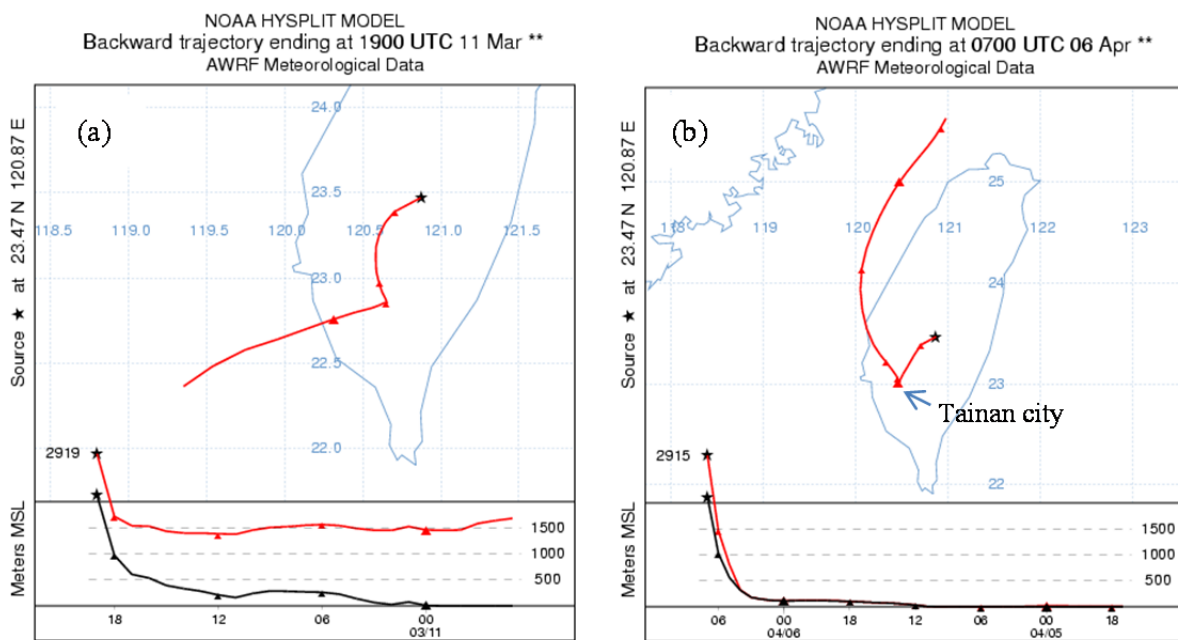


**Fig. 8.** The backward trajectories originating from Mt. Lulin from (a) 39 hours before 3:00 LST March 12 2010 (b) 25 hours before 15:00 LST April 6 2010. The black star indicates the location of Mt. Lulin. The red and black lines indicate the trajectory and terrain height, respectively.

39 hours before the air parcel arrived at Mt. Lulin is described. The air parcel arriving at Mt. Lulin at 15:00 LST on April 6 possibly originated from the ground (Fig. 6(m)). The backward trajectory showed the air parcel to move southwestward along the coast over Taiwan Strait and turn to land at the coast of central Taiwan at 14:00 LST on April 5 (Fig. 8(b)). At 17:00 LST on April 5, the air parcel entered land and continued to move southeastward for approximately 9 hours. The air parcel became stagnant from 02:00 LST to 08:00 LST on April 6 in Tainan City located in southwestern Taiwan. The stagnant point is right at the bottom of the CMR. Then, the air parcel moved along the CMR northeastward at 08:00 LST on April 6 via the valley wind. After 7 h, the air parcel arrived at Mt. Lulin.

The simulated pressure, temperature, and water vapor were quite stable in the air parcel over the sea (Fig. 10(a)). At 14:00 LST on April 5, the concentration of various pollutants, such as  $\text{NH}_3$ ,  $\text{NO}_x$ ,  $\text{SO}_2$ , VOC,  $\text{NO}_3^-$ , and  $\text{NH}_4^+$ , increased evidently after 18:00 LST on April 5 since the air parcel entered land and mixed with urban/industrial pollution (Figs. 10(b)–10(e)). At 6 h when the air parcel was stagnant, the proportions of  $\text{NO}_3^-$  and  $\text{NH}_4^+$  in  $\text{PM}_{2.5}$  simultaneously increased. The concentrations of the urban representative pollutants  $\text{NO}_3^-$  and  $\text{NH}_4^+$  also increased consistently. However, the concentrations of  $\text{SO}_4^{2-}$  and OM remained almost constant. Therefore, the increase in  $\text{PM}_{2.5}$  was mainly attributed to the increase in the concentrations of  $\text{NO}_3^-$  and  $\text{NH}_4^+$  (Fig. 10(f)). After 08:00 LST on April 6, the air parcel moved northeastward and climbed the CMR. During this movement, the proportions and concentrations of  $\text{NO}_3^-$  and  $\text{NH}_4^+$  simultaneously decreased. By contrast, the proportions and concentrations of PAN, PANX, SULF, and OM increased. The increase in OM included primary and secondary OC.

However, the secondary OC produced by the VOC emitted by the forest in the mountains was not a major composition but the anthropogenic primary OC from urban traffic in this study, since the OC from biogenic emissions (AORGBT in Fig. 10(e)) was much less than the OC from primary emission (AORGPAT in Fig. 10(e)). The OM and EC concentrations and proportions increased, although the concentrations and proportions of  $\text{NO}_3^-$  and  $\text{NH}_4^+$  in the air parcel decreased during this movement because the air parcel was far from the urban area. This phenomenon occurred because the air parcel was influenced by the high-altitude BB plume as the plume approached Mt. Lulin.

#### **High-Altitude BB Plume Affected the Air Quality on the Ground**

The BB plume from Southeast Asia could impact the air quality on the ground in Southern Taiwan was firstly proposed by Tsai *et al.* (2012). Later, Yen *et al.* (2013) suggested that a cold surge causes a downward flow that drags high-altitude BB pollutants to the ground and found that a cold surge accompanied with a cold front or a cold surge that occurred one or two days after a cold front passed Taiwan on March 9, 16, and 25 and on April 2, 7, and 13 in 2010 resulted in the deterioration of the air quality at the Hengchun ground site. Therefore, Yen *et al.* (2013) suggested that the high-altitude BB plume is the cause of occasional air quality deterioration in Hengchun. In the present study, the downward motion in the cold surge may transport the high-altitude BB plume to the ground. However, the BB plume involved in the long-range transport contained small amounts of  $\text{SO}_2$  and  $\text{NO}_x$  because these substances are likely converted into  $\text{SO}_4^{2-}$  and  $\text{NO}_3^-$  (Chuang *et al.*, 2015). The observed monthly  $\text{SO}_2$  and  $\text{NO}_x$  concentrations

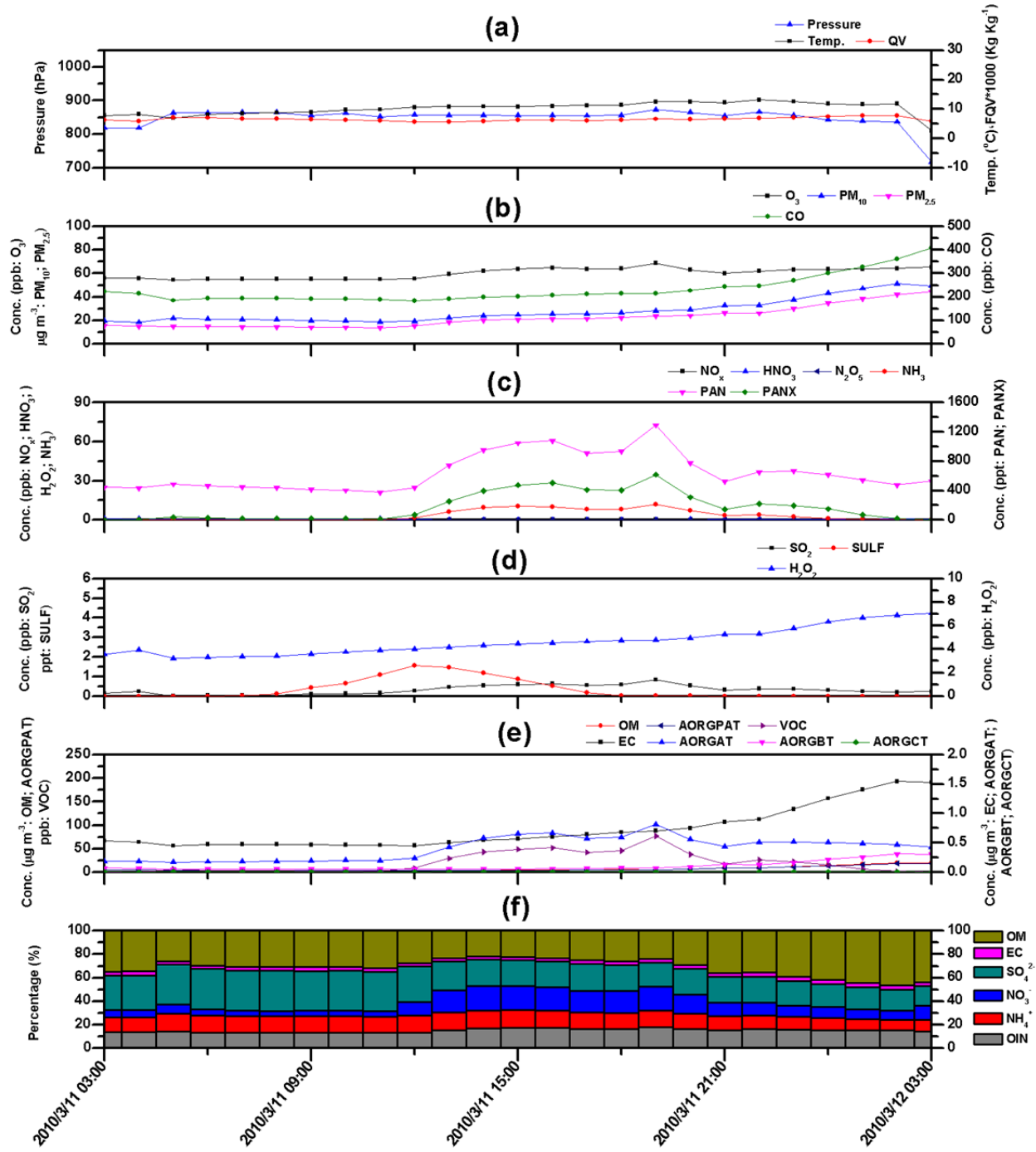


**Fig. 9.** The chemical evolution of meteorological variables and chemical species in the BB parcel which moved along the trajectory in Fig. 8(a) and arrived at Mt. Lulin at 03:00 LST on March 12, 2010 (Temp: temperature; QV: water vapor mixing ratio; PAN: peroxy acetyl nitrate; PANX: peroxy propionyl nitrate (PPN) + peroxy methacryloyl nitrate (MPAN); AORGPAT: anthropogenic primary organic aerosol; AORGAT: anthropogenic secondary organic aerosol; AORGBT: biogenic secondary organic aerosol; AORGCT: cloud secondary organic aerosol).

at Mt. Lulin from March to April 2010 were  $0.6 \pm 0.3$  and  $2.1 \pm 1.0$  ppb, respectively, and these values were less than those detected in Hengchun ( $\text{SO}_2 > 5$  ppb,  $\text{NO}_x > 10$  ppb) in the six events. Furthermore, the level of  $\text{SO}_2$  and  $\text{NO}_x$  is obviously caused by the anthropogenic sources (Chiu *et al.*, 2005). Therefore, BB was not the major source that induced those events. Instead, the major source was accompanied

with the front ahead of the Asian outflow, which passed Taiwan in the form of lower stratified flow (Lin *et al.*, 2004; Chuang *et al.*, 2008; Lin *et al.*, 2012). Therefore, cold surge is a minor cause. We also observed that a cold front passed Taiwan on March 2 and 21 and on April 15, 23, and 27. The following cold surge did not cause an increase in the concentrations of the simulated or observed pollutants

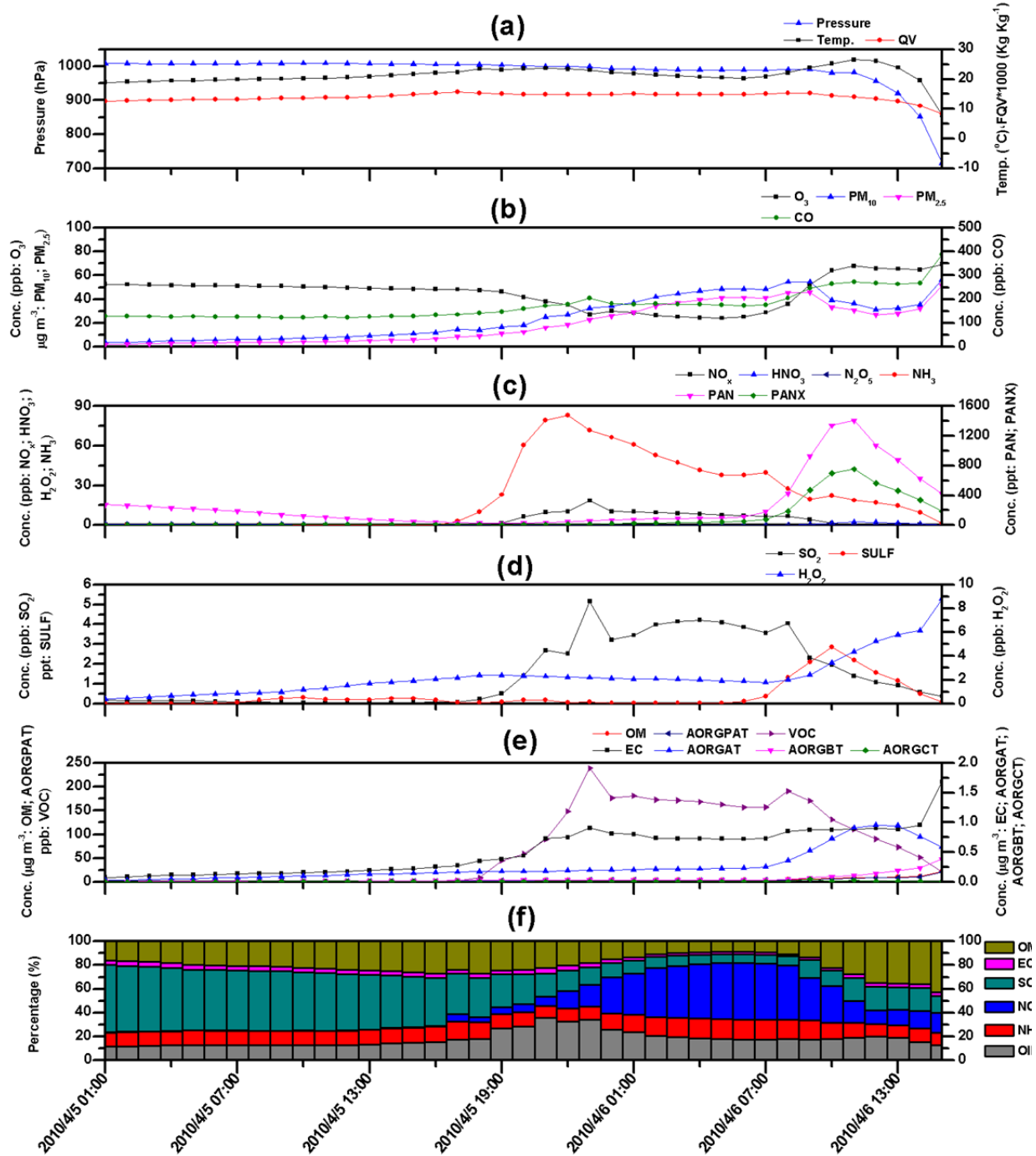


**Fig. 10.** These figures are similar as Fig. 9 but for the air parcel which moved along the trajectory in Fig. 8(b) and arrived at Mt. Lulin at 15:00 LST on April 6, 2010.

because a high-altitude BB plume did not move to Taiwan on these days. Therefore, front/cold surge is not indicative if the high-altitude BB plume likely influenced the air quality on the ground. Instead, the anthropogenic pollutants accompanying the Asian continent outflow cause the air quality in Taiwan to deteriorate (Lin *et al.*, 2004; Chuang *et al.*, 2008; Lin *et al.*, 2012).

We compared the observations and simulations at the Hengchun site. Fig. 11 shows that CO,  $PM_{10}$ , and  $PM_{2.5}$  were underestimated, but  $O_3$  was satisfactory. The performances

of CO and PM were unsatisfactory because the 5 km resolution cannot resolve complex terrain near Hengchun and the overestimated wind speed led to underestimation of CO and PM when these two pollutants were from local pollution. However, the  $O_3$  was well simulated no matter when it was from the background winter monsoon or local pollution. Moreover, the horizontal resolution of domain 3 (Fig. 1) in this simulation was only 5 km, which could not accurately resolve the geography near Hengchun because the Hengchun Peninsula is only 15 km in width. The resolved

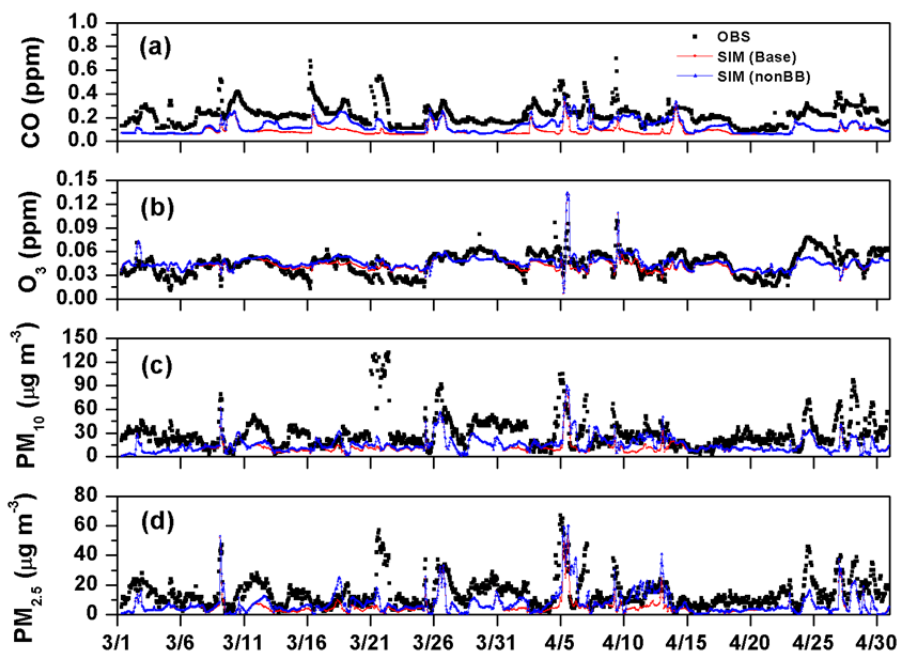


**Fig. 11.** The time variation of (a) CO, (b) O<sub>3</sub>, (c) PM<sub>10</sub>, (d) PM<sub>2.5</sub> for observation and simulations at Hengchun site.

terrain height is less than 300 m, which is much lower than the nearby hills of 500 m to 700 m in height. This discrepancy caused the overestimation of wind speed, resulting in the underestimation of pollutant concentrations. The other minor reasons causing underestimation could be the use of INTEX-B anthropogenic emission inventory, which was based on 2006 data, and the exclusion of dust emission. For example, the dust event that occurred on March 19 to 21, 2010, was the most severe dust storm event in the last ten years (Bian *et al.*, 2011). Therefore, the simulated PM<sub>10</sub> and PM<sub>2.5</sub> were underestimated in the present study.

The impact of BB still can be resolved from the difference of sensitivity test with and without BB pollution emission. The contribution can then be estimated as the impact of BB to the measurements. The influence of BB was apparently > 20% on March 9, 12 to 24, and 31 and on April 1 to 14, 16 to 18, and 27 for CO; March 9, 12 to 22, 31, and April 1 to 14 for PM<sub>10</sub>; March 3 to 7, 12 to 24, 28, 31, and April 1 to 20 for PM<sub>2.5</sub>; and April 5 to 6 and 10 to 13 for O<sub>3</sub> at the Hengchun site (Fig. 11). In the two months of the simulations, the contributions of CO, O<sub>3</sub>, PM<sub>10</sub>, and PM<sub>2.5</sub> from BB at Hengchun were 15.0%, 6.6%, 13.0%, and 24.0%, respectively.

## CONCLUSIONS

This study aimed to discuss the phenomena of the BB plume that approached Taiwan in March and April 2010. The CMAQ model was used to observe the movement of the BB plume and the chemical evolution of the pollutants along the moving trajectories. This study also described the mechanism by which the BB plume influenced the high-altitude Mt. Lulin site in central Taiwan and the Hengchun ground site in the southern tip of Taiwan.

For PM<sub>2.5</sub> at Mt. lulin, the simulation results showed that

the contribution of the BB plume was approximately 60% to 90% when the BB plume apparently reached Mt. Lulin. While for the two-month simulation period, the average contributions of BB and non-BB emissions were 53% and 47%, respectively. This discrepancy indicated that the contribution from the non-BB emissions should be considered at Mt. Lulin. This study also showed that three mechanisms could explain the influence of the high-altitude BB plume on the air quality on the ground when the BB plume approached the windward side of CMR: (1) the subsidence in anticyclone, (2) the mixing in the boundary layer, and (3) the downward flow in the cold surge from Asia. However, the third mechanism was overstated in the past.

This study also analyzed two events (12 March 2010, 3:00 LST and 6 April 2010, 15:00 LST) in the chemical evolution of the pollutants in the high-altitude BB plume and the near-ground air parcel along the moving trajectories before these substances reached Mt. Lulin. In the first event, the BB plume was influenced by the near-surface pollutants because of the turbulent diffusion in the boundary layer when the high-altitude BB plume entered the land on the west of Taiwan. The concentrations of primary and secondary pollutants, such as PAN, PANX, NH<sub>3</sub>, SO<sub>2</sub>, VOC, NO<sub>3</sub><sup>-</sup>, increased. When approaching Mt. Lulin, the BB plume began to climb along the slope of the CMR at approximately half the height of the CMR (1,500 m in this event) and arrived at Mt. Lulin via terrain lifting. The concentrations of the pollutants increased when the BB plume was near Mt. Lulin because of the compression by the CMR.

In the second event, the air parcel was transported upward by the valley wind from the bottom of mountains. When the air parcel was moving upward the CMR, the concentrations and proportions of NO<sub>3</sub><sup>-</sup> and NH<sub>4</sub><sup>+</sup> decreased, whereas the concentrations and proportions of PAN, PANX, SULF, and OM increased. The increase in the concentration of OM was

not caused by the production of VOCs emitted by the forest in the mountains near Mt. Lulin but emitted by the urban traffic. The biogenic OC was only a minor composition of OC in this event. When the air parcel approached Mt. Lulin, the concentrations and proportions of OM and EC increased, this result indicated that the air parcel was influenced by the high-altitude BB plume.

A sensitivity test was conducted to describe the impact of high-altitude BB on the Hengchun surface site. In March and April 2010, the contributions of BB on CO, O<sub>3</sub>, PM<sub>10</sub>, and PM<sub>2.5</sub> were 15.0%, 6.6%, 13.0%, and 24.0%, respectively. In particular, the impact of CO and PM was > 20% for more than half of the days in the two months.

Even without the blocking by the CMR, high altitudes could influence the air quality near the ground through the subsidence in the anticyclone, the mixing in the boundary layer, and the downward flow in the cold surge. We hope that this description of the impact of the SEA BB on downwind areas will prompt researchers to further investigate this topic.

## ACKNOWLEDGMENTS

We would like to express our gratitude to the Taiwan National Science Council (NSC 100-2111-M-008-017, NSC 101-2111-M-008-005, NSC 102-2111-M-008-010, and MOST 103-2111-M-008-005). We would also like to thank the Taiwan Environmental Protection Agency for the data obtained at Lulin Atmospheric Background Station (LABS). We acknowledge the US National Centers for Environmental Prediction (NCEP) for providing the Final Operation Global Analysis (FNL) data and the Taiwan Central Weather Bureau and Data Bank of Atmospheric Research (DBAR) managed by the National Taiwan University for the meteorological maps.

## REFERENCES

- Air Sciences, Inc. (2002). Fire Emission Inventory for the WRAP Region – Phase II, Preared for the Western Governors Association/WRAP by Air Sciences, Inc., Denver, CO.
- Andreae, M.O. and P. Merlet, P. (2001). Emission of trace gases and aerosols from biomass burning. *Global Biogeochem. Cycles* 15: 955–966.
- Baltensperger, U., Gäggeler, H.W., Jost, D.T., Lugauer, M., Schwikowski, M. and Weingartner, E. (1997). Aerosol climatology at the high-alpine site Jungfraujoch, Switzerland. *J. Geophys. Res.* 102: 18707–19715.
- Bian, H., Tie, X., Cao, J., Ying, Z., Han, S. and Xue, Y. (2011). Analysis of a severe dust storm event over China: Application of the WRF-Dust model. *Aerosol Air Qual. Res.* 11: 419–428.
- Byun, D. and Schere, K.L. (2006). Review of the governing equations, computational algorithms, and other components of the models-3 community multiscale air quality (CMAQ) modeling system. *Appl. Mech. Rev.* 59: 51–77.
- Carnuth, W. and Trickl, T. (2000). Transport studies with the IFU three-wavelength aerosol lidar during the VOTALP Mesolcina experiment. *Atmos. Environ.* 34: 1425–1434.
- Chan, L.Y., Chan, C.Y., Liu, H.Y., Christopher, S., Oltmans, S.J. and Harris, J.M. (2000). A case study on the biomass burning in southeast Asia and enhancement of tropospheric ozone over Hong Kong. *Geophys. Res. Lett.* 27: 1479–1482.
- Chang, S.C., Lee, W.J., Wang, L.C., Lin, N.H. and Chang-Chien, G.P. (2013). Influence of the Southeast Asian biomass burnings on the atmospheric persistent organic pollutants observed at near sources and receptor site. *Atmos. Environ.* 78: 184–194.
- Chiu, K.H., Sree, U., Tseng, S.H., Wu, C.H. and Lo, J.G., (2005). Differential optical absorption spectrometer measurement of NO<sub>2</sub>, SO<sub>2</sub>, O<sub>3</sub>, HCHO and aromatic volatile organics in ambient air of Kaohsiung Petroleum Refinery in Taiwan. *Atmos. Environ.* 39: 941–955.
- Chuang, M.T., Fu, J.S., Jiang, C.J., Chan, C.C., Ni, P.C. and Lee, C.T. (2008). Simulation of long-range transport aerosols from the Asian Continent to Taiwan by a southward Asian high-pressure system. *Sci. Total Environ.* 406: 168–179.
- Chuang, M.T., Lee, C.T., Lin, N.H., Chou, C.C.K., Wang, J.L., Sheu, G.R., Chang, S.C., Wang, S.H., Huang, H., Cheng, H.W., Weng, G.H., Lai, S.Y., Hsu, S.P. and Chang, Y.J. (2014). Carbonaceous aerosols in the air masses transported from Indochina to Taiwan: Long-term observation at Mt. Lulin. *Atmos. Environ.* 89: 507–516.
- Chuang, M.T., Fu, J.S., Lin, N.H., Lee, C.T., Gao, Y., Wang, S.H., Sheu, G.R., Hsiao, T.C., Wang, J.L., Yen, M.C., Lin, T.H., Thongboonchoo, N. and Chen, W.C. (2015). Simulating the transport and chemical evolution of biomass burning pollutants originating from Southeast Asia during 7-SEAS/2010 Dongsha experiment. *Atmos. Environ.* 112: 294–305.
- Frioud, M., Mitev, V., Matthey, R., Häberli, C.H., Richner, H., Werner, R. and Vogt, S. (2003). Elevated aerosol stratification above the Rhine Valley under strong anticyclonic conditions. *Atmos. Environ.* 37: 1785–1797.
- Fu, J.S., Hsu, N.C., Gao, Y., Huang, K., Li, C., Lin, N.H. and Tsay, S.C. (2012). Evaluating the influences of biomass burning during 2006 BASE-ASIA: A regional chemical transport modeling. *Atmos. Chem. Phys.* 12: 3837–3855.
- Guenther, A.B., Jiang, X., Heald, C.L., Sakulyanontvittaya, T., Duhl, T., Emmons, L.K. and Wang, X. (2012). The Model of Emissions of Gases and Aerosols from Nature version 2.1 (MEGAN2.1): An extended and updated framework for modeling biogenic emissions. *Geosci. Model Dev.* 5: 1471–1492.
- Houyoux, M. and Vukovich, J. (1999). Updates to the Sparse Matrix Operator Kernel Emissions (SMOKE) Modeling System and Integration with Models-3, Presented at The Emissions Inventory: Regional Strategies for the Future Conference, Journal of Air and Waste Management Association, Raleigh, NC.
- Huang, K., Fu, J.S., Hsu, N.C., Gao, Y., Dong, X., Tsay, S.C. and Lam Y.F. (2013). Impact assessment of biomass burning on air quality in Southeast and East Asia during BASE-ASIA. *Atmos. Environ.* 78: 291–302.

- Hyer, E.J. and Chew, B.N. (2010). Aerosol transport model evaluation of an extreme smoke episode in Southeast Asia. *Atmos. Environ.* 44: 1422–1427.
- King, M. D., Kaufman, Y. J., Menzel, W. P., and Tanre, D. (1997). Remote sensing of cloud, aerosol, and water vapor properties from the moderate resolution imaging spectrometer (MODIS). *IEEE Trans. Geosci. Remote Sens.* 30: 2–27.
- Lau, L.J. (2012). The Long-term Economic Growth of Taiwan. Institute of Global Economics and Finance, Chinese University of Hong Kong, Working Paper No. 13.
- Lavin, K.S. and Hageman, K.J. (2013). Contributions of long-range and regional atmospheric transport on pesticide concentrations along a transect crossing a mountain divide. *Environ. Sci. Technol.* 47: 1390–1398.
- Lee, C.T., Chuang, M.T., Lin, N.H., Wang, J.L., Sheu, G.R., Chang, S.C., Wang, S.H., Huang, H., Chen, H.W., Liu, Y.L., Weng, G.H., Lai, H.Y. and Hsu, S.P. (2011). The enhancement of PM<sub>2.5</sub> mass and water-soluble ions of biosmoke transported from Southeast Asia over the Mountain Lulin site in Taiwan. *Atmos. Environ.* 45: 5784–5794.
- Lee, C.T., Ram, S.S., Nguyen, D.L., Chou, C.C.K., Chang, S.Y., Lin, N.H., Chang, S.C., Hsiao, T.C., Sheu, G.R., Ou-Yang, C.F., Chi, K.H., Wang, S.H. and Wu, X.C. (2016a). Aerosol chemical profile of near-source biomass burning smoke in Sonla, Vietnam during 7-SEAS campaigns in 2012 and 2013. *Aerosol Air Qual. Res.* 16: 2603–2617.
- Lee, J., Hsu, N.C., Bettenhausen, C., Sayer, A.M., Seftor, C.J., Jeong, M.J., Tsay, S.C., Welton, E.J., Wang, S.H. and Chen, W.N. (2016b). Evaluating the height of biomass burning smoke aerosols retrieved from synergistic use of multiple satellite sensors over Southeast Asia. *Aerosol Air Qual. Res.* 16: 2831–2842.
- Lin, C.Y., Liu, S.C., Chou, C.C., Liu, T.H., Lee, C.T., Yuan, C.S., Shiu, C.J. and Young, C.Y. (2004). Long-range transport of Asian dust and air pollutants to Taiwan. *Terrae Atmos. Oceanic Sci.* 15: 759–784.
- Lin, C.Y., Zhao, C., Liu, X., Lin, N.H. and Chen, W.N. (2014). Modelling of long-range transport of Southeast Asia biomass-burning aerosols to Taiwan and their radiative forcings over East Asia. *Tellus Ser. B* 66: 23733.
- Lin, C.Y., Chou, C.C.K., Wang, Z., Lung, S.C., Lee, C.T., Yuan, C.S., Chen, W.N., Chang, S.Y., Hsu, S.C., Chen, W.C. and Liu, S.C. (2012). Impact of different transport mechanisms of Asian dust and anthropogenic pollutants to Taiwan. *Atmos. Environ.* 60: 403–418.
- Lin, N.H., Tsay, S.C., Maring, H.B., Yen, M.C., Sheu, G.R., Wang, S.H., Chi, K.H., Chuang, M.T., Ou-Yang, C.F., Fu, J.S., Reid, J.S., Lee, C.T., Wang, L.C., Wang, J.L., Hsu, C.N., Sayer, A.M., Holben, B.N., Chu, Y.C., Nguyen, X.A., Sopajaree, K., Chen, S.J., Cheng, M.T., Tsuang, B.J., Tsai, C.J., Peng, C.M., Schnell, R.C., Conway, T., Chang, C.T., Linw, K.S., Tsai, Y.I., Lee, W.J., Chang, S.C., Liu, J.J., Chiang, W.L., Huang, S.J., Lin, T.H. and Liu, G.R. (2013). An overview of regional experiments on biomass burning aerosols and related pollutants in Southeast Asia: From BASE-ASIA and the Dongsha Experiment to 7-SEAS. *Atmos. Environ.* 78: 1–19.
- Lin, Y.C., Lin, C.Y. and Hsu, W.T. (2010). Observations of carbon monoxide mixing ratios at a mountain site in central Taiwan during the Asian biomass burning season. *Atmos. Res.* 95: 270–278.
- Marinoni, A., Cristofanelli, P., Laj, P., Duchi, R., Calzolri, F., Decesari, S., Sellegrini, K., Vuillermoz, E., Verza, G.P., Villani, P. and Bonasoni, P. (2010). Aerosol mass and black carbon concentrations, a two year record at NCO-P (5079 m, Southern Himalayas). *Atmos. Chem. Phys.* 10: 8551–8562.
- Matsui, H., Koike, M., Kondo, Y., Oshima, N., Moteki, N., Kanaya, Y., Takami, A. and Irwin, M. (2013). Seasonal variations of Asian black carbon outflow to the Pacific: Contribution from anthropogenic sources in China and biomass burning sources in Siberia and Southeast Asia. *J. Geophys. Res.* 118: 9948–9967.
- Nam, J., Wang, Y., Luo, C. and Chu, D.A. (2010). Trans-Pacific transport of Asian dust and CO: Accumulation of biomass burning CO in the subtropics and dipole structure of transport. *Atmos. Chem. Phys.* 10: 3297–3308.
- Ou-Yang, C.F., Lin, N.H., Sheu, G.R., Lee, C.T. and Wang, J.L. (2012). Seasonal and diurnal variations of ozone at a high-altitude mountain baseline station in East Asia. *Atmos. Environ.* 46: 279–288.
- Perrone, M.G., Larsen, B.R., Ferrero, L., Sangiorgi, G., Gennaro, G.D., Udisti, R., Zangrando, R., Gambaro, A., and Bolzacchini, E. (2012). Sources of high PM<sub>2.5</sub> concentrations in Milan, Northern Italy: Molecular marker data and CMB modelling. *Sci. Total Environ.* 414: 343–355.
- Reid, J.S., Hyer, E.J., Prins, E.M., Westphal, D.L., Zhang, J., Wang, J., Christopher, S.A., Curtis, C.A., Schmidt, C.C., Eleuterio, D.P., Richardson, K.A. and Hoffman, J.P. (2009). Global monitoring and forecasting of biomass-burning smoke: Description of and lessons from the fire locating and modeling of burning emissions (FLAMBE) program. *IEEE J. Sel. Top. Appl. Earth Obs. Remote Sens.* 2: 144–162.
- Sayer, A.M., Hsu, N.C., Hsiao, T.C., Pantina, P., Kuo, F., Ou-Yang, C.F., Holben, B.N., Janjai, S., Chantara, S., Wang, S.H., Loftus, A.M., Lin, N.H. and Tsay, S.C. (2016). In-situ and remotely-sensed observations of biomass burning aerosols at Doi Ang Khang, Thailand during 7-SEAS/BASELInE 2015. *Aerosol Air Qual. Res.* 16: 2786–2801.
- Sheu, G.R., Lin, N.H., Wang, J.L., Lee, C.T., Ou Yang, C.F. and Wang S.H. (2010). Temporal distribution and potential sources of atmospheric mercury measured at a high-elevation background station in Taiwan. *Atmos. Environ.* 44: 2393–2400.
- Tsai, J.H., Huang, K.L., Lin, N.H., Chen, S.J., Lin, T.C., Chen, S.C., Lin, C.C., Hsu, S.C. and Lin, W.Y. (2012). Influence of an Asian dust storm and Southeast Asia biomass burning on the characteristics of seashore atmospheric aerosols in Southern Taiwan. *Aerosol Air Qual. Res.* 12: 1105–1115.
- TWEPA (2011). National Air Emission Trends Inventory

- System Management and Review (2). Taiwan EPA Report, EPA-100-FA11-03-D047, in Chinese.
- USEPA (2007). Guidance on the Use of Models and Other Analyses for Demonstrating Attainment of Air Quality Goals for Ozone, PM<sub>2.5</sub> and Regional Haze, EPA-454/B-07e002.
- Wai, K.M. and Tanner, P.A. (2014). Recent springtime regional CO variability in Southern China and the adjacent ocean: Anthropogenic and biomass burning contribution. *Aerosol Air Qual. Res.* 14: 21–32.
- Wang, J., Ge, C., Yang, Z., Hyer, E.J., Reid, J.S., Chew, B.N., Mahmud, M., Zhang, Y. and Zhang, M. (2013). Mesoscale modeling of smoke transport over the Southeast Asian Maritime Continent: Interplay of sea breeze, trade wind, typhoon, and topography. *Atmos. Res.* 122: 486–503.
- Wang, W., Bruyère, C., Duda, M., Dudhia, J., Gill, L., Lin, H.C., Michalakes, J., Rizvi, S., Zhang, X., Beezley, J.D., Coen, J.I. and Mandel, J. (2012). ARW Version 3 Modeling System User'S Guide. Mesoscale & Microscale Meteorology Division, National Center for Atmospheric Research (July 2010, Last Updated January 2012).
- Willmott, C.J. (1981). On the validation of models. *Phys. Geo.* 2: 184–194.
- Yen, M.C., Peng, C.M., Chen, T.C., Chen, C.S., Lin, N.H., Tzeng, R.Y., Lee, Y.A. and Lin, C.C. (2013). Climate and weather characteristics in association with the active fires in northern Southeast Asia and spring air pollution in Taiwan during 2010 7-SEAS/Dongsha Experiment. *Atmos. Environ.* 78: 35–90.
- Zhang, J.I., Reid, J.S., Westphal, D.L., Baker, N. and Hyer, E.J. (2008). A system for operational aerosol optical depth data assimilation over global oceans. *J. Geophys. Res.* 113: D10208.
- Zhang, Q., Streets, D.G., Carmichael, G.R., He, K.B., Huo, H., Kannari, A., Klimont, Z., Park, I.S., Reddy, S., Fu, J.S., Chen, D., Duan, L., Lei, Y., Wang, L.T. and Yao, Z.I. (2009). Asian emissions in 2006 for the NASA INTEX-B mission. *Atmos. Chem. Phys.* 9: 5131–5153.
- Zhang, Y.M., Zhang, X.Y., Sun, J.Y., Hu, G.Y., Shen, X.J., Wang, Y.Q., and Wang, T.T. (2014). Chemical composition and mass size distribution of PM<sub>1</sub> at an elevated site in central east China. *Atmos. Chem. Phys.* 14: 12237–12249.

Received for review, July 23, 2015

Revised, November 2, 2015

Accepted, December 3, 2015